Protein dynamics studied on myoglobin

Fritz Parak and Klaus Achterhold

Physik-Department E17, Technische Universität München, D-85747 Garching, Germany

Two methods of inelastic scattering of synchrotron radiation were used to measure the dynamics of myoglobin in the temperature range from $T = 60$ K to 300 K. The inelastic Rayleigh scattering of metmyoglobin was analyzed by delayed elastic nuclear forward scattering of an iron foil. This yields averaged information on all phonons within the sample. The mean square displacement of the atoms due to this dynamics is $\langle x^2\rangle/T = 2.1 \cdot 10^{-4}$ Å^2 K^{-1} on average. Complementary information was obtained by phonon assisted nuclear scattering on deoxymyoglobin. This method selects the phonons coupling to the iron atom in the active center of the protein. The mean square displacement of the iron was measured to be $\langle x^2\rangle/T = 0.6 \cdot 10^{-4}$ Å^2 K^{-1}. The results are in agreement with Mössbauer absorption experiments in the low temperature range. Above 200 K the results allow one to distinguish between harmonic and quasidiffusive dynamics within the protein. A comparison with Raman spectroscopy is made.

1. Introduction

Proteins perform a large number of functions in biology. Even the smallest proteins are large molecules with a highly organized architecture. Although the knowledge of the 3-dimensional structure of a protein is indispensable for an understanding of its function, this knowledge is not enough. Structural fluctuations open and close channels through which ligands or substrates enter and leave the active center of a protein molecule. Structural changes between different conformations, i.e., ligated or unligated, are of great importance. In the case of myoglobin, the oxygen ligand has first to diffuse through the protein matrix before it can bind at the iron. However, the average structure as obtained by X-ray structure analysis shows no open channel [1,2]. Each binding process involves movements of atoms of the protein matrix. A physical understanding of the "protein dynamics" is one important field of biophysics.

From many proteins myoglobin was selected as a model compound for the physical investigation of protein dynamics. Myoglobin is often called the "hydrogen atom of biophysics". This indicates that one hopes to learn from this molecule basic physical pictures which can be generalized for several other proteins. For the investigation, a large number of physical techniques has been applied. The rebinding of CO after flash photolysis of CO ligated myoglobin yielded basic insights into the structural distributions of protein molecules [3]. This technique was used in numerous investigations and still gives many new concepts (compare, e.g., [4]). The structure and the structural distributions were studied by X-ray structure analysis from

room temperature down to 40 K [5–7]. X-ray structure analysis at low temperatures was also able to resolve intermediate structures between the ligated and the unligated conformation [8–10]. Mössbauer spectroscopy and optical spectroscopy gave a deep insight into structural relaxations [11,12]. The equilibrium fluctuations of myoglobin within one conformation were mainly investigated by Mössbauer spectroscopy [13,14], Rayleigh scattering of Mössbauer radiation [15–17] and incoherent neutron scattering [18]. In this contribution we want to show that even the first experiments on Rayleigh and nuclear scattering of synchrotron radiation analyzed by the Mössbauer effect give valuable information on the dynamics of myoglobin. The inelastic scattering of synchrotron radiation has proved to be an appropriate tool for the investigation of phonons in matter. We compare this new technique with other techniques and discuss the results in the context of the general picture of structural fluctuations in proteins.

2. Myoglobin; sample preparation

Myoglobin is a protein with a molecular weight of about 17800 Da. We used myoglobin from horse heart and sperm whale respectively. Both consist of 153 residues and one heme group of protoporphyrin IX with an iron in the center. The difference in 19 residues between horse heart and sperm whale myoglobins is unimportant for the present investigation, the overall structure is nearly identical [19]. The amino acid chain is organized in 8 α-helices numbered A to H connected by short interhelical loops (see figure 1(a)). The 3-dimensional folding yields a globular structure with a diameter of about 30 Å. The function of myoglobin is to store the oxygen delivered by the blood until it is needed by the organism. The O_2 binds in the active site of the protein at the sixth coordination of the iron. The protein matrix influences the electronic configuration of the iron in such a way that binding and releasing of the ligand becomes easily reversible. The iron is linked to the protein moiety via the nitrogen N_ε of the histidine F8 (His93) in the F helix (see figure 1(b)). This is the only bond of the heme to the protein matrix. Four coordinations of the iron are occupied by the N-atoms of the protoporphyrin IX. The remaining 6th coordination is either empty in deoxymyoglobin (Mbdeoxy) or occupied by oxygen (MbO_2) or other ligands like CO (MbCO) or H_2O (Mbmet). In Mbdeoxy the iron is in the Fe(II) high spin state. It is shifted out of the heme plane by about 0.4 Å towards the histidine F8 [10]. Binding a ligand the iron moves more or less into the heme plane. In H_2O ligated Mbmet the iron to heme plane distance is 0.1 Å and the iron is in the Fe(III) high spin state.

We used two samples. Sample A contained Mbmet of horse heart, where the lyophilized material was kept in a constant humidity atmosphere until it reached a water content of 0.4 g H_2O/g protein. This material was bought from Sigma and used without any further purification. Sample B consisted of a large number of small sperm whale Mbdeoxy crystals randomly oriented. It was enriched in ^{57}Fe as described by [13]. The crystals were grown according to [20]. The crystallographic unit cell

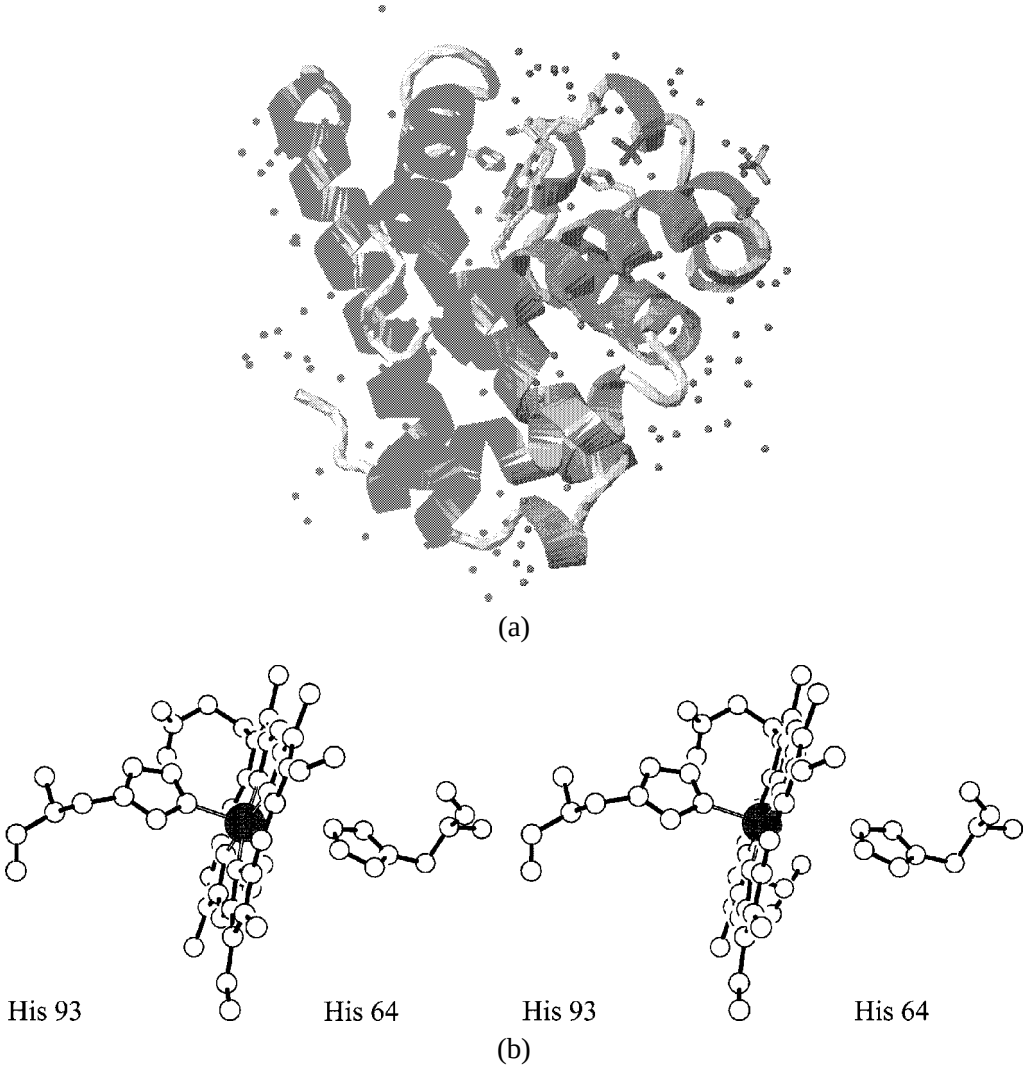

Figure 1. (a) The backbone of myoglobin with 170 crystallographically visible water molecules. The 8 α-helices are connected by interhelical loops. The heme plane with the iron is visible in the middle upper part. (b) Stereoview of the heme plane with the proximal histidine His93 and the distal histidine His64. The iron is marked in black.

contains two molecules of myoglobin. In addition, there are about 840 water molecules within a unit cell [21]. This gives a water content of the crystals of 0.4 g H_2O/g protein. The water content of sample A was adjusted to give the same value. 120 mg of the samples, respectively, were sealed in a vacuum tight plastic sample holder with mylar windows of 40 μm thickness allowing the beam to pass and the scattered radiation to leave the sample. The length of the beam path through the sample was 10 mm with a cross-section of 0.3×1 mm^2.

3. Experimental method

We briefly summarize the most important features of the experiments and refer to [22] for a detailed description of the beamline and further articles in this issue for a more detailed discussion of the experimental techniques [23]. The experiments were performed at the beamline ID18 of the ESRF, Grenoble. With the synchrotron working in the 16 bunch mode X-ray pulses of 100 ps were provided every 176 ns. A Si(1 1 1) double monochromator followed by a Si(4 2 2)/Si(9 7 5) nested high resolution monochromator yielded an energy bandwidth of 4.4 meV at an energy in the region of 14.4 keV. This energy was varied in the range of ± 70 meV in steps of 0.8 meV around the Mössbauer resonance. Two avalanche photodiodes with a time resolution of about 1 ns were used to detect the scattered radiation. A time delayed intensity between 10 and 150 ns after the end of the X-ray flash indicated a nuclear resonant scattering at a ^{57}Fe nucleus. Mössbauer nuclei are either within an iron foil used as energy analyzer or within the sample (compare figures 2(a), (b)). If the X-ray flash does not include the Mössbauer resonance energy, there is no resonant absorption in ^{57}Fe nuclei. All scattered radiation is detected instantaneously. Inelastic scattering events provide a possibility to compensate an energy mismatch of the incoming radiation with respect to the Mössbauer transition. The rate of delayed radiation at a certain energy mismatch is then proportional to the number of dynamical modes, e.g., phonons of that energy, which can be annihilated or created in the scattering process.

Two slightly different experimental set-ups were used. The set-up in figure 2(a) allows the analysis of the inelastic scattering of synchrotron radiation by the electrons of the sample [24]. All phonons within the sample may contribute to change the energy of the scattered radiation. The energy analysis of the radiation scattered by the myoglobin sample is performed by an ^{57}Fe metal foil (A2) of 7.5 μm thickness. If the energy of the scattered radiation fits within the width of the Mössbauer resonance it is elastically forward scattered by the ^{57}Fe foil with delay into an avalanche photodiode (APD1). Inelastic scattering within the analyzer foil can also shift the energy of the radiation to the Mössbauer resonance, resulting in additional delayed reemission. In contrast to the former case, this radiation is emitted into the full solid angle and is, due to the high factor of internal conversion ($\alpha = 8.18$), mainly of 6.4 keV energy. An electronic threshold allows the detection of the 14.4 keV forward scattered radiation but discriminates against the 6.4 keV fluorescence. In addition, an aluminium foil of 300 μm thickness in front of the detector mainly absorbs the 6.4 keV radiation. The high factor of internal conversion in connection with the better efficiency of the APD for the 6.4 keV radiation would otherwise distort the measurement of the phonon spectrum of the myoglobin sample by the inelastic scattering of the analyzer. The momentum transfer to the sample is determined by the scattering angle. Due to the distance of the photodiode APD1 to the sample (3.5 mm) and the area of the detector (10×10 mm^2) momentum transfers between $|\vec{k}| = 2.5$ Å^{-1} and 14.3 Å^{-1} are accepted. Counting rates were about 1 per second in the elastic peak maximum with a background of 0.018 s^{-1} measured with beam shutters closed. The energy ref-

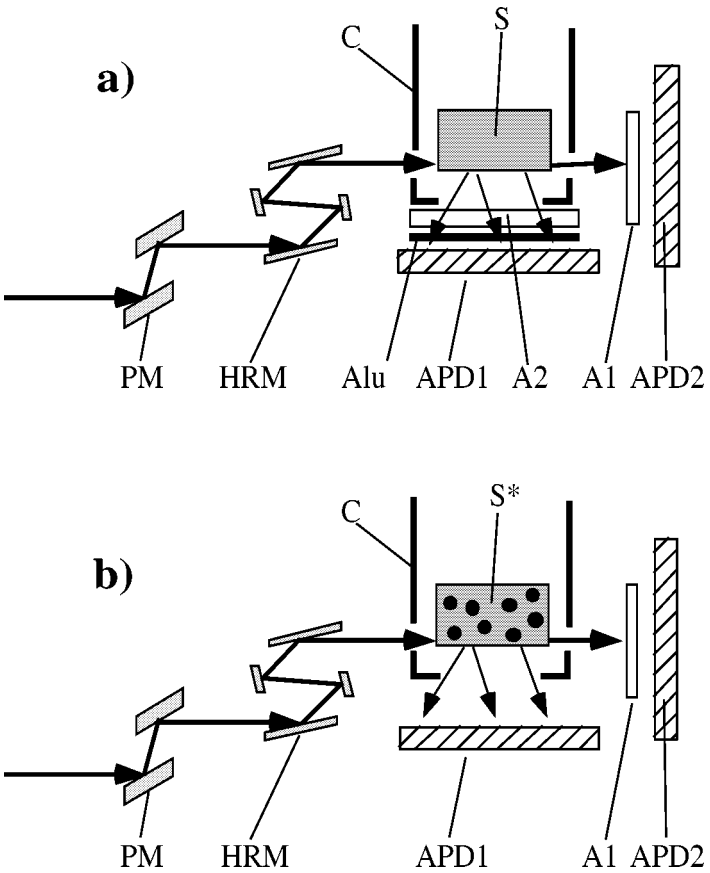

Figure 2. Sketch of the experiments. PM: Si(1 1 1)/Si(1 1 1) double premonochromator; HRM: Si(4 2 2)/Si(9 7 5) high resolution nested monochromator; APD1/2: avalanche photodiodes; A1: iron metal foil enriched in ^{57}Fe for energy reference; C: closed cycle refrigerator. (a) S: Mbmet not enriched in ^{57}Fe (sample A); Alu: aluminium foil of 300 μm thickness; A2: iron metal analyzer foil of 7.5 μm thickness, enriched in ^{57}Fe. (b) S*: Mbdeoxy crystals enriched in ^{57}Fe (sample B).

erence is performed in an additional iron metal foil A1 where the radiation which passed the sample can be elastically forward scattered with delay into the avalanche photodiode APD2. This practically happens only if the energy covers the Mössbauer resonance. The overall energy resolution is that of the high resolution monochromator.

In the set-up shown in figure 2(b) all time delayed radiation comes from Mössbauer decays of ^{57}Fe nuclei within the sample [25,26]. Obviously, an energy mismatch of the incoming radiation can only be compensated by phonons coupling to the iron atoms of the sample. One obtains phonon assisted nuclear resonant scattering. The momentum transfer is that of the Mössbauer quantum ($|\vec{k}| = 7.3$ Å^{-1}) independently of the scattering geometry. In this set-up the detector APD1 accepts 14.4 keV Mössbauer radiation as well as the 6.4 keV fluorescence X-rays from in-

ternal conversion. Due to internal conversion the delayed radiation consists of about 11% of 14.4 keV quanta and 89% of 6.4 keV K_α fluorescence radiation of iron. The counting rates were about 2 s^{-1} in the elastic peak maximum. Also in this set-up the analyzer A1 serves as an energy reference and yields the energy resolution of the equipment.

4. Results and discussion

Figure 3(a) shows the inelastic nuclear scattering spectrum of the enriched Mb-deoxy crystals (sample B) measured at room temperature [27]. The spectrum is normalized by setting the first moment of the spectrum to the recoil energy of the iron nucleus $E_R = 1.94$ meV [28]. This procedure circumvents the problem of the large change in nuclear absorption within the resonance and out of it [26]. The elastic peak measured in the forward direction (compare figure 3(a)) represents the resolution of the equipment. It is removed by a least squares procedure in order to extract the phonon density of states. As a restraint the remaining inelastic intensities are forced to be connected by the Boltzmann factor between intensities of opposite energies. This is valid for harmonic oscillations. It can further be assumed that a Debye-like density of states is responsible for the low energy inelastic scattering. The area of the remaining, purely inelastic spectrum is then equal to $1 - f$, where f is the Lamb–Mössbauer factor. It can be shown [29] that the elastic plus inelastic scattering spectrum $S(E)$ is connected with the one phonon scattering function by

$$FT\{S(E)\} = f e^{FT\{S_1(E)\}}, \tag{4.1}$$

where *FT* denotes the Fourier transformation. This extraction of the one phonon scattering $S_1(E)$ is called the Fourier-log method. Via $S_1(E)$ one obtains the density of states $g(E)$ of phonons coupling to the iron shown in eq. (4.2) and figure 3(b):

$$g(E) = S_1(E)\left(1 - e^{-E/(k_B t)}\right) \cdot \frac{E}{E_R}. \tag{4.2}$$

For the analysis of the spectrum it was assumed that the measured intensity comes from a convolution of the phonon spectrum with the symmetric energy resolution of the equipment. No correction for an asymmetry of the energy resolution as described in [26] was necessary. The distinct maximum between the energies 25 to 40 meV in figure 3(a) is seen in the density of states as at least three resolved lines (figure 3(b)). The comparison with a resonance Raman spectrum of Mbdeoxy in solution [30] shows good agreement of the frequency positions at 27 and 38 meV. The line at 27 meV corresponding to 220 cm^{-1} (100 $cm^{-1} \cong 12.4$ meV) is known to be an iron histidine (F8) stretching frequency [31]. The broad line at about 30–36 meV ($\sim$282 cm^{-1}) and the line at 65 meV seem to be Raman silent. The Raman line at 46 meV represents a vibration coupling only weakly to the iron atom. A sharp line at 52 meV is due to the quartz sample holder of the Raman experiment (marked q

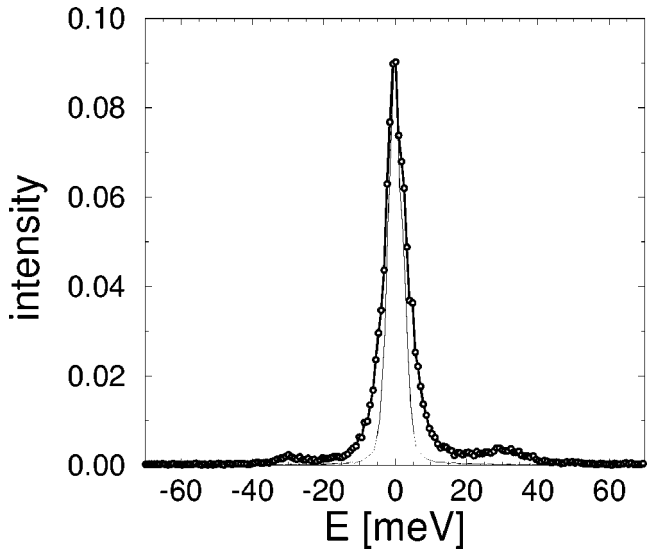

(a)

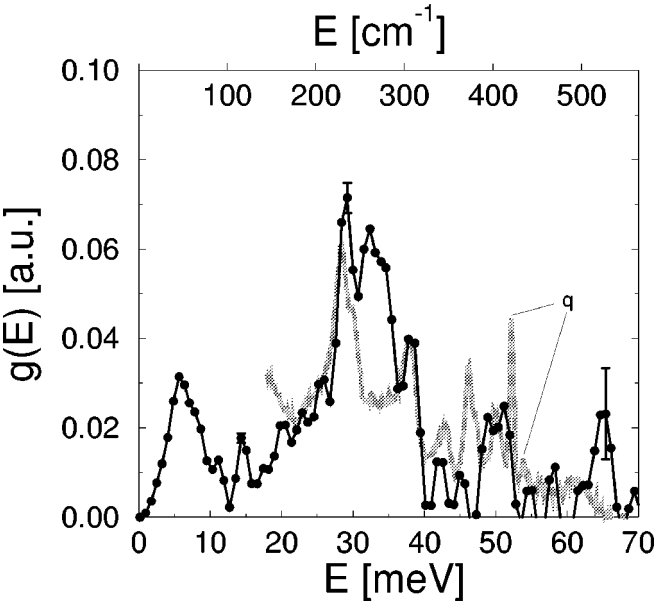

(b)

Figure 3. (a) Open circles: inelastic nuclear scattering spectrum of Mbdeoxy crystals at room temperature [27]. The energy E is counted with respect to the Mössbauer resonance energy of ^{57}Fe. Beside the elastic line at zero energy, only scattering from phonon modes coupling selectively to the iron atom are seen. Thin line: resolution of the monochromator device measured in the forward direction. (b) Closed circles: density of phonon states coupling to the iron in Mbdeoxy crystals measured at room temperature. The density is extracted from the data given in figure 3(a) with the Fourier-log method outlined in the text. Thick line: resonance Raman spectrum of Mbdeoxy at 4 K [30]. The lines marked by q originate from the quartz sample holder.

in figure 3(b)). These latter features show the advantage of inelastic nuclear scattering: The extracted density of states yields all and solely the iron vibrations. The Raman intensity depends strongly on the polarizability (see eq. (5.6)). The intensities of the nuclear inelastic scattering depend only on the density of vibronic states $g(E)$. A comparison with the method of Raman spectroscopy is given in the last section.

The inelastic X-ray scattering of hydrated myoglobin allows a study of the density of all phonons in the sample. The integral of each scattering spectrum is normalized to unity. For this purpose it is assumed that the cross-section for scattering and absorption of the X-rays is taken to be constant within the energy band of about ± 100 meV. In contrast to the phonon assisted nuclear scattering, a distribution of momentum transfers to the sample has to be taken into account. This was done by analyzing the scattering geometry and absorption within the sample. Due to the large scattering angles the scattering can be taken as incoherent in a good approximation. The dependence of the total, elastic and inelastic, scattering intensity from the scattering angle was calculated with the aid of the known protein and water structure [21]. The normalized spectra are fitted by a least squares procedure yielding a density of phonon states for each spectrum. Results at two temperatures are shown in figure 4 as solid lines. We compare the extracted phonon density with a spectrum obtained by incoherent neutron scattering [32] in figure 5. Up to now the statistics of the measurement is not sufficient to resolve deviations. At least at low energy transfers, the total phonon spectrum is rather insensitive to the differences of hydrogen motions and the motions of the C, N and O atoms.

The occupation of each phonon state is given by the Bose–Einstein statistics resulting in a temperature dependent mean square displacement

$$\left\langle x^2 \right\rangle = \int_0^\infty \frac{\hbar^2}{mE} \left(\frac{1}{2} + \frac{1}{\mathrm{e}^{E/(k_\mathrm{B}T)} - 1} \right) g(E)\, \mathrm{d}E. \tag{4.3}$$

In the case of nuclear resonant scattering m is the mass of the Mössbauer nucleus. For the case of Rayleigh scattering we used for m a mean mass averaged over the atoms of the sample weighted by the square of the number of electrons for each atom. In this harmonic model, for sufficiently high temperatures, $\langle x^2 \rangle$ is proportional to the temperature and a fit to the phonon spectrum should yield a linear dependence of $\langle x^2 \rangle$. The results at four temperatures are shown in figure 6 as open squares. The error bar is due to an uncertainty of ± 1 mm in the distance of the detector to the sample. The dashed line with a slope of $\langle x^2 \rangle / T = 2.1 \cdot 10^{-4}$ Å^2/K is a linear regression.

Mössbauer spectroscopy has been used for many years to study protein dynamics of myoglobin. Rayleigh scattering of Mössbauer radiation yields mean square displacements averaged over all atoms in the molecule [33]. Modes of motions which couple to the heme iron reveal themselves in the Mössbauer absorption spectra by a decrease of the nuclear absorption probability. Moreover, the Mössbauer absorption spectra of myoglobin show additional broad lines besides the usual Lorentzians if the temperature is higher than 180 K. The area of the narrow Lorentzians is proportional

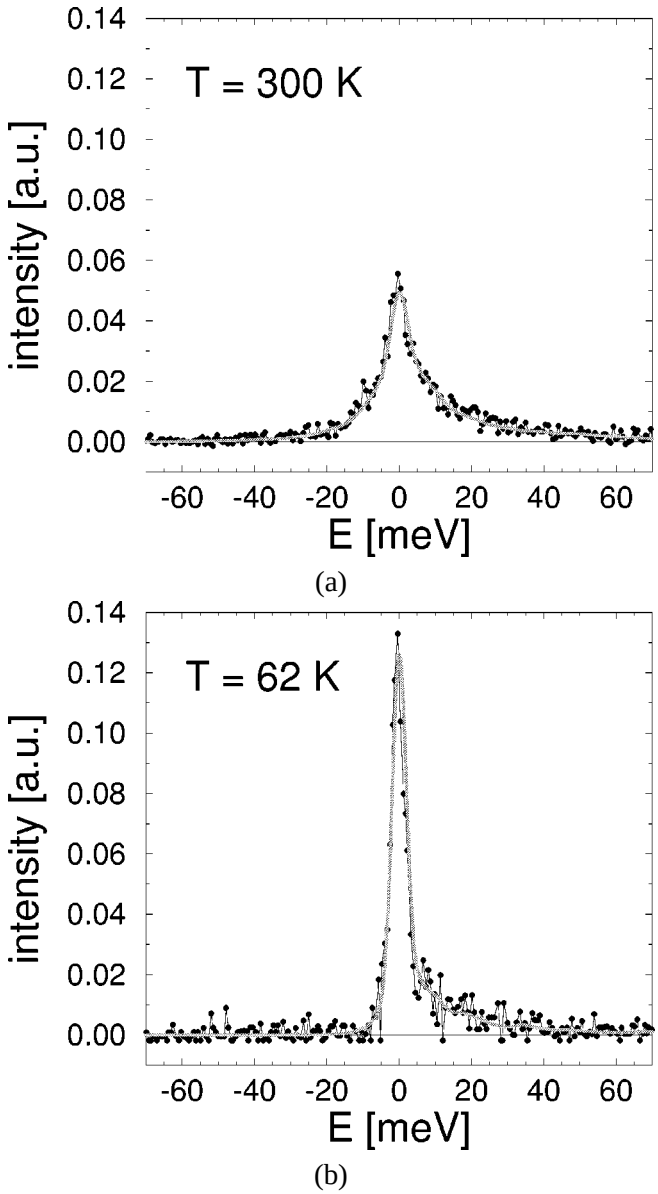

Figure 4. Inelastic Rayleigh scattering spectrum of hydrated Mbmet at temperatures of (a) 300 K and (b) 62 K. The energy refers to the Mössbauer resonance energy of ^{57}Fe within the analyzer foil. The inelastic spectrum is due to all phonons of the sample.

to the Lamb–Mössbauer factor $f = \exp(-k^2\langle x^2\rangle)$, where k equals $2\pi/\lambda$ ($\lambda = 0.86$ Å in the case of ^{57}Fe). The mean square displacement, $\langle x^2\rangle$, of iron in Mbdeoxy crystals is shown in figure 7 as closed circles [14]. It increases linearly with temperature below $\approx$180 K. This increase is in good agreement with normal mode calculations taking into

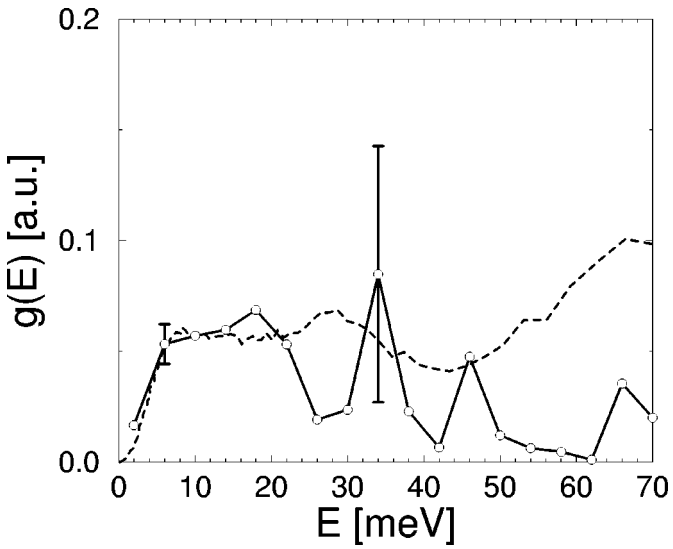

Figure 5. Density of states of all phonons in hydrated Mbmet. Open circles with error bars are the mean of the fit results to spectra at 300, 189 and 124 K. The broken line shows the result from neutron scattering [32]. Due to the large error bars of the synchrotron measurement a comparison between the results of the different methods is possible only in the low energy part ($E < 20$ meV).

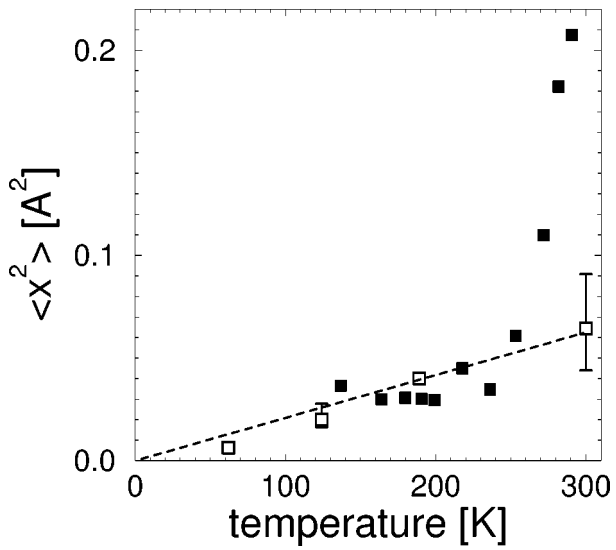

Figure 6. Temperature dependence of the mean square displacement $\langle x^2 \rangle$ in myoglobin. Closed squares: $\langle x^2 \rangle$ average of all atoms in Mbmet crystals measured by inelastic Rayleigh scattering of Mössbauer radiation with a ^{57}CoCr Mössbauer source [15]. Open squares: $\langle x^2 \rangle$ of all atoms in hydrated Mbmet measured by inelastic Rayleigh scattering of synchrotron radiation. Dashed straight line: fit of a linear temperature dependence to the Mbmet data.

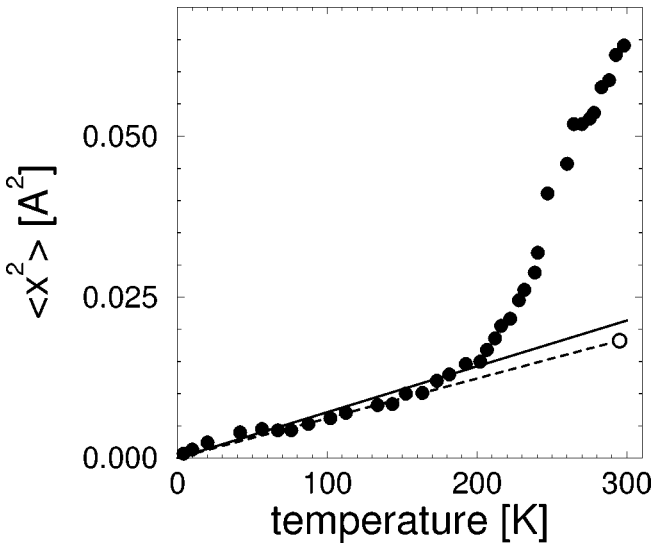

Figure 7. Closed circles: $\langle x^2 \rangle$ of the iron atom in Mbdeoxy crystals measured by Mössbauer absorption [14]. Open circle: harmonic $\langle x^2 \rangle$ at $T = 295$ K due to phonons coupling to the iron in Mbdeoxy crystals as measured with the inelastic nuclear scattering of synchrotron radiation. Dashed line: indication of a harmonic temperature dependence of the iron mean square displacement. Solid line: mean square displacement of the iron obtained by a normal mode analysis [34].

account all modes which couple to the iron [34]. However, at higher temperatures there occurs a dramatic increase of the $\langle x^2 \rangle$-values with temperature. Correlated, additional broad absorption lines appear in the Mössbauer spectrum. This gives the following picture of protein dynamics: At low temperatures a protein molecule essentially performs harmonic motions which can be described by normal modes. At a characteristic temperature, T_c, of about 180 K a new type of motions starts to contribute. The shape of the Mössbauer spectrum indicates a bound diffusion of molecular segments with respect to each other. The diffusive motions are limited in space by the binding forces within the molecule. This type of motions can be described by the Brownian oscillator [35] or by a jump diffusion model with a time distribution according to, for instance, Cole and Davidson [36].

We now want to see if this picture is compatible with our experiments with synchrotron radiation. It has been discussed in [37] that the areas of the spectra shown in figure 4 are independent of temperature. Nevertheless, the shape of the energy spectrum of inelastic X-ray scattering changes strongly with temperature. An increasing temperature shifts intensity from the central peak to the phonon part of the spectrum. An estimation showed that an average mean square displacement calculated from this phonon part increases linearly with temperature up to 300 K (see figure 6). The temperature dependence of the inelastic scattering is in good agreement with a harmonic approach up to room temperature. It also agrees with an estimate of an average $\langle x^2 \rangle^{\mathrm{RSMR}}$-value determined by Rayleigh scattering of Mössbauer radia-

tion below 200 K. However, it should be emphasized that such averaged mean square displacements do not allow a very specific physical interpretation. The inelastic scattering does not explain the strong additional increase of the mean square displacement seen in the RSMR experiments above 250 K and at the iron position at about 180 K. Mössbauer absorption spectroscopy shows that the increase at the iron position stems from quasi-diffusive motions in a limited region. Such motions cause quasi-elastic scattering. The involved energy change is very small in comparison to inelastic scattering. Mössbauer spectra give neV to μeV as the order of magnitude at the position of the iron. In the synchrotron experiment the energy resolution was only 4.4 meV. This means that a quasi-elastic process seen by Mössbauer absorption spectroscopy with an energy resolution of some neV cannot be separated in the synchrotron experiments. The quasi-elastic scattering is hidden in the central elastic peak of figure 4. One may now argue that we compare an experiment which is sensitive to all modes of motions with a Mössbauer experiment where only modes of motions are measured which couple to the iron. However, the temperature dependence of the phonon spectrum has also been measured with synchrotron radiation using the set-up in figure 2(b). Phonon assisted nuclear resonance gives similar information as Mössbauer absorption spectroscopy. Again a linear temperature dependence from 40 to 295 K was obtained (still unpublished). The open circle in figure 7 is the mean square displacement at 295 K calculated with eq. (4.3) and the density of states of the phonons coupling to the iron shown in figure 3(b). The straight dashed line indicates the linear temperature dependence of $\langle x^2 \rangle$ with a slope of $\langle x^2 \rangle / T = 0.6 \cdot 10^{-4}$ Å^2/K.

5. Competition with other experimental methods

Inelastic scattering of synchrotron radiation analyzed by Mössbauer absorption is a new technique where results complementary to incoherent neutron scattering and Raman scattering have been obtained. Here, we briefly discuss the principal differences.

Incoherent neutron scattering. This method gives similar results as our first set-up. It allows the determination of density of states for phonons [38,39]. However, due to the large incoherent structure factor of the hydrogen nucleus, the inelastic scattering involves only motions, which are coupled to the H atoms. Motions like rotations of methyl groups contribute. In contrast, the scattered intensity of synchrotron radiation is proportional to the square of the number of electrons of the different atoms. Therefore, it gives a high weight to motions which couple to the C, N and O atoms or heavier ones of the myoglobin molecule. The contribution of the H atoms is practically negligible.

Raman scattering. It is generally used for the investigation of specific vibrations in proteins. Modes of motions coupling to the heme iron in myoglobin were up to now mainly investigated by resonant Raman spectroscopy. The π electronic system of the heme is excited with visible lasers and vibrational modes which influence the π–π^*

transition are enhanced. For a review see [40]. We try in the following to clarify the principal differences of these experimental methods. Essentially, they are due to the different energies of the radiations.

Raman experiments are performed in the frequency range of visible light. The frequency of the radiation used in the synchrotron radiation experiments is more than 3 orders of magnitude larger. In the first case one is well below the electron resonance energies in atoms and molecules, while in the second case one is above those energies. In the following we give a rough estimation for the differences in the scattering process. The electric field of X-rays or light induces a time-dependent dipole moment $\vec{p}(t)$ within the atoms and molecules of a sample. The amplitude of the scattered radiation in the equatorial plane of the dipole is

$$\vec{E}_S(t) = \frac{1}{R}\frac{1}{4\pi\varepsilon_0}\left(\frac{\omega_i}{c}\right)^2 \vec{p}(\omega_i, t), \tag{5.1}$$

where R is a distance which is large compared to the dipole dimension, ε_0 is the dielectric constant, c the velocity of light, and ω_i the frequency of the incoming radiation. In the simplest approximation, one can explain the frequency dependence of the scattered radiation with one electron bound to the nucleus. The equation for a forced motion in a harmonic potential leads to the dipole moment

$$\vec{p}(\omega_i, t) = \frac{e_0^2}{m_{\mathrm{e}}(\omega_0^2 - \omega_i^2)}\vec{E}\left(\vec{r}_{\mathrm{e}}, t\right) = \alpha\vec{E}. \tag{5.2}$$

Here ω_0 is the electron resonance frequency and m_{e} and e_0 are the mass and the charge of the electron, respectively; $\vec{r}_{\mathrm{e}}$ is its position. Equation (5.2) introduces the polarizability α. The incoming wave at the position $\vec{r}_{\mathrm{e}}$ is given by

$$\vec{E}\left(\vec{r}_{\mathrm{e}}, t\right) = \vec{E}_0 \mathrm{e}^{\mathrm{i}(\vec{k}\vec{r}_{\mathrm{e}} - \omega_i t)}, \tag{5.3}$$

where $\vec{k}$ is the wave vector of the incoming radiation.

The limit of $\omega_i \ll \omega_0$, valid for scattering of light, yields $\alpha \propto 1/\omega_0^2$, independent of the frequency of the incoming light but dependent on the resonance frequency ω_0 of the oscillating electron. This resonance frequency is influenced by the position $\vec{r}$ of the atom considered in the molecule, which depends on time:

$$\vec{r}(t) = \left\langle \vec{r} \right\rangle + \vec{u}(t), \tag{5.4}$$

where $\langle \vec{r} \rangle$ is the mean atomic position and $\vec{u}(t)$ its dynamic deviation from this position. The dependence of the polarizability on vibrational amplitudes can be expanded in a Taylor series to give

$$\alpha(u) = \alpha_0 + \left(\frac{\partial\alpha}{\partial u}\right)_0 u + \cdots + \frac{1}{n!}\left(\frac{\partial^n\alpha}{\partial u^n}\right)_0 u^n + \cdots, \tag{5.5}$$

where the index 0 stands for the mean position $\langle \vec{r} \rangle$. The first term gives the elastic Rayleigh scattering, whereas the second gives the first order Raman scattering and

so on. If the polarizability is a symmetric function of the normal mode amplitude this mode will give no first order Raman effect. Only a mode which changes the polarizability yields a Raman scattering.

If the vibrational amplitude

$$\hat{u}(t) = \left(\frac{\hbar}{2m\omega_V}\right)^{1/2}\left(\hat{a}(t) + \hat{a}^{+}(t)\right)$$

is written with the creation and annihilation operators $\hat{a}(t) = \hat{a}\mathrm{e}^{-\mathrm{i}\omega_V t}$ and $\hat{a}^{+}(t) = \hat{a}^{+}\mathrm{e}^{\mathrm{i}\omega_V t}$ the first order Raman scattering is

$$\begin{aligned}\vec{E}_S(t) &= \frac{1}{R}\frac{1}{4\pi\varepsilon_0}\left(\frac{\omega_i}{c}\right)^2\left(\alpha_0 + \left(\frac{\partial\alpha}{\partial u}\right)_0 u\right)\vec{E}(\vec{r},t)\\ &= \frac{1}{R}\frac{1}{4\pi\varepsilon_0}\left(\frac{\omega_i}{c}\right)^2\vec{E}_0\mathrm{e}^{\mathrm{i}\vec{k}\vec{r}}\\ &\quad\times\left(\alpha_0\mathrm{e}^{-\mathrm{i}\omega_i t} + \left(\frac{\partial\alpha}{\partial u}\right)_0\left(\frac{\hbar}{2m\omega_V}\right)^{1/2}\left(\hat{a}\mathrm{e}^{-\mathrm{i}(\omega_i+\omega_V)t} + \hat{a}^{+}\mathrm{e}^{-\mathrm{i}(\omega_i-\omega_V)t}\right)\right). \quad (5.6)\end{aligned}$$

After Fourier transformation one obtains the well-known central elastic Rayleigh line at ω_i and the Stokes and anti Stokes side bands at a distance $\pm\omega_V$ to ω_i. It should be noted that the time dependence of $\vec{r}(t)$ in the term $\mathrm{e}^{\mathrm{i}\vec{k}\vec{r}}$ in eq. (5.6) gives no contribution because the wavelength of the light is very long in comparison to $u(t)$. However, $\vec{r}(t)$ becomes important for X-rays.

In the X-ray case the limit $\omega_i \gg \omega_0$ applies and the polarizability becomes

$$\alpha = -\frac{e_0^2}{m_\mathrm{e}\omega_i^2}. \quad (5.7)$$

It no longer depends on the electron resonance frequency. The scattered amplitude according to eq. (5.1) becomes

$$\vec{E}_S(t) = -\frac{1}{R}\frac{1}{4\pi\varepsilon_0}\frac{e_0^2}{m_\mathrm{e}c^2}\vec{E}_0\mathrm{e}^{\mathrm{i}(\vec{k}\vec{r}-\omega_i t)}. \quad (5.8)$$

Inelastic effects enter by the time dependence of $\vec{r}(t)$ according to eq. (5.4) because $u(t)$ is now in the order of the wavelength λ of the scattered radiation. Using the Gaussian approximation and the cumulant expansion [41,42] one gets for the scattered intensity

$$\begin{aligned}I(\vec{k},t) = \left|\vec{E}_S(t)\right|^2 &= \left(\frac{1}{R}\,\frac{\sin\theta}{4\pi\varepsilon_0}\,\frac{e_0^2}{m_\mathrm{e}c^2}\vec{E}_0\right)^2\mathrm{e}^{-\mathrm{i}\omega_i t}\mathrm{e}^{-1/2\langle(\vec{k}[\vec{u}(0)-\vec{u}(t)])^2\rangle}\\ &= \left(\frac{1}{R}\,\frac{\sin\theta}{4\pi\varepsilon_0}\,\frac{e_0^2}{m_\mathrm{e}c^2}\vec{E}_0\right)^2\mathrm{e}^{-\mathrm{i}\omega_i t}\mathrm{e}^{-k^2\langle x^2\rangle}\sum_{n=0}^{\infty}\frac{1}{n!}k^{2n}\left\langle x(0)x(t)\right\rangle^n. \quad (5.9)\end{aligned}$$

Here $x(t)$ is the component of $\vec{u}(t)$ in the direction of the transferred momentum $\vec{k}$ and it is assumed that $\langle x(0)^2\rangle = \langle x(t)^2\rangle = \langle x^2\rangle$. The summation runs over the elastic line (for $n = 0$) and the multiple phonon scattering for $n = 1, 2, \ldots$. No interference of the scattering by different electrons is considered here for simplicity. Taking again the time dependent creation and annihilation operators for the harmonic oscillator $\hat{a}(t) = \hat{a}\mathrm{e}^{-\mathrm{i}\omega_V t}$ and $\hat{a}^+(t) = \hat{a}^+\mathrm{e}^{\mathrm{i}\omega_V t}$ one gets inelastic lines shifted with respect to the central elastic line. For a number of modes with different energies and all combinations of different modes one ends up with the inelastic scattering spectrum. For clarity it should be written here just for one mode and one phonon scattering as

$$I(\vec{k},t) = \left(\frac{1}{R}\frac{\sin\theta}{4\pi\varepsilon_0}\frac{e_0^2}{m_\mathrm{e}c^2}\vec{E}_0\right)^2 \mathrm{e}^{-\mathrm{i}\omega_i t}\mathrm{e}^{-k^2\langle x^2\rangle} \times \left(1 + \frac{\hbar k^2}{2m\omega_V}\frac{1}{1-\mathrm{e}^{-\hbar\omega_V/(k_\mathrm{B}T)}}\left\{\mathrm{e}^{\mathrm{i}\omega_V t} + \mathrm{e}^{-\hbar\omega_V/(k_\mathrm{B}T)}\mathrm{e}^{-\mathrm{i}\omega_V t}\right\}\right). \quad (5.10)$$

The first term of the sum written in curved brackets yields the inelastic line shifted by $E = \hbar\omega_V$ for phonon creation. The phonon annihilation line is shifted by $E = -\hbar\omega_V$ and weakened by the detailed balance factor $\mathrm{e}^{-E/(k_\mathrm{B}T)}$. This is the so-called inelastic Rayleigh scattering.

Beside the discussed effect the difference in frequency of light and X-rays has another consequence. The momentum of light in the wavelength region of a few hundred nm is small compared with the momentum of phonons in the first Brillouin zone of crystals. The conservation of momentum demands that only vibrations with wave vectors K practically zero are excited in the first order Raman effect. In contrast, the momentum of X-rays is so large that all K values in the Brillouin zone can be transferred. For our first set-up this allows in principle a determination of the density of states as a function of K. At present, the experiments integrate over the whole Brillouin zone due to a lack in intensity. The density of states is then dominated by the Van Hove singularities, where the gradient of a phonon branch vanishes.

Acknowledgements

This work was supported by the Bundesministerium für Bildung, Wissenschaft, Forschung und Technologie.

References

[1] M.F. Perutz and F.S. Mathews, J. Mol. Biol. 21 (1966) 199.
[2] D.A. Case and M. Karplus, J. Mol. Biol. 132 (1979) 343.
[3] R.H. Austin, K.W. Beeson, L. Eisenstein, H. Frauenfelder and I.C. Gunsalus, Biochem. 14 (1975) 5355.
[4] G.U. Nienhaus, J.R. Mourant and H. Frauenfelder, Proc. Nat. Acad. Sci. USA 89 (1992) 2902.
[5] H. Frauenfelder, G.A. Petsko and D. Tsernoglou, Nature 280 (1979) 558.

[6] H. Hartmann, F. Parak, W. Steigemann, G.A. Petsko, D. Ringe Ponzi and H. Frauenfelder, Proc. Nat. Acad. Sci. USA 79 (1982) 4967.
[7] F. Parak, H. Hartmann, K.D. Aumann, H. Reuscher, G. Rennekamp, H. Bartunik and W. Steigemann, European Biophys. J. 15 (1987) 237.
[8] T.Y. Teng, V. Srajer and K. Moffat, Nat. Struct. Biol. 1 (1994) 701.
[9] I. Schlichting, J. Berendzen, G.N. Phillips and R.M. Sweet, Nature 317 (1996) 808.
[10] H. Hartmann, S. Zinser, P. Komninos, R.T. Schneider, G.U. Nienhaus and F. Parak, Proc. Nat. Acad. Sci. USA 93 (1996) 7013.
[11] V.E. Prusakov, J. Steyer and F.G. Parak, Biophys. J. 68 (1995) 2524.
[12] D.C. Lamb, A. Ostermann, V.E. Prusakov and F.G. Parak, European Biophys. J. 27 (1998) 113.
[13] F. Parak and H. Formanek, Acta Cryst. A 27 (1971) 573.
[14] F. Parak, E.W. Knapp and D. Kucheida, J. Mol. Biol. 161 (1982) 177.
[15] Yu.F. Krupyanskii, F. Parak, V.I. Goldanskii, R.L. Mössbauer, E.E. Gaubmann, H. Engelmann and I.P. Suzdalev, Z. Naturforsch. 37c (1982) 57.
[16] G.U. Nienhaus, H. Hartmann and F. Parak, Hyp. Interact. 47 (1989) 299.
[17] F. Parak, K. Achterhold, H. Hartmann, J. Heinzl, E. Huenges and G.U. Nienhaus, Hyp. Interact. 71 (1992) 1319.
[18] S. Cusack and W. Doster, Biophys. J. 58 (1990) 243.
[19] S.V. Evans and G.D. Brayer, J. Mol. Biol. 213 (1990) 885.
[20] J.C. Kendrew and A.G. Parrish, Proc. Roy. Soc. Ser. A 238 (1957) 305.
[21] M. Schmidt, F. Parak and G. Corongiu, Internat. J. Quant. Chem. 59 (1996) 263.
[22] R. Rüffer and A.I. Chumakov, Hyp. Interact. 97/98 (1996) 589.
[23] A.I. Chumakov and W. Sturhahn, this issue, section V-1.1.
[24] A.I. Chumakov, A.Q.R. Baron, R. Rüffer, H. Grünsteudel, H.F. Grünsteudel and A. Meyer, Phys. Rev. Lett. 76 (1996) 4258.
[25] M. Seto, Y. Yoda, S. Kikuta, X.W. Zhang and M. Ando, Phys. Rev. Lett. 74 (1995) 3828.
[26] W. Sturhahn, T.S. Toellner, E.E. Alp, X. Zhang, M. Ando, Y. Yoda, S. Kikuta, M. Seto, C.W. Kimball and B. Dabrowski, Phys. Rev. Lett. 74 (1995) 3832.
[27] C. Keppler, K. Achterhold, A. Ostermann, U. van Bürck, W. Potzel, A.I. Chumakov, R. Rüffer and F. Parak, European Biophys. J. 25 (1997) 221.
[28] H.J. Lipkin, Ann. Phys. 9 (1960) 332.
[29] D.W. Johnson and J.C.H. Spence, J. Phys. D 7 (1974) 771.
[30] M. Sassaroli, S. Dasgupta and D.L. Rousseau, J. Biol. Chem. 261 (1986) 13704.
[31] D.L. Rousseau and J.M. Friedman, in: *Biological Applications of Raman Spectroscopy*, Vol. 3, ed. T.G. Spiro (Wiley, New York, 1988) p. 133.
[32] M. Settles and W. Doster, in: *Biological Macromolecular Dynamics*, eds. S. Cusack, H. Büttner, M. Ferrand, P. Langan and P. Timmins (Adenine Press, Schenectady, 1996) p. 3.
[33] Yu.F. Krupyanskii, V.I. Goldanskii, G.U. Nienhaus and F. Parak, Hyp. Interact. 53 (1990) 59.
[34] B. Melchers, E.W. Knapp, F. Parak, L. Cordone, A. Cupane and M. Leone, Biophys. J. 70 (1996) 2092.
[35] F. Parak and E.W. Knapp, Proc. Nat. Acad. Sci. USA 81 (1984) 7088.
[36] I. Chang, H. Hartmann, Yu. Krupyanskii, A. Zharikov and F. Parak, Chem. Phys. 212 (1996) 221.
[37] K. Achterhold, C. Keppler, U. van Bürck, W. Potzel, P. Schindelmann, E.-W. Knapp, B. Melchers, A.I. Chumakov, A.Q.R. Baron, R. Rüffer and F. Parak, European Biophys. J. 25 (1996) 43.
[38] S.W. Lovesey, in: *Theory of Neutron Scattering from Condensed Matter*, eds. R.J. Elliott, J.A. Krumhansl, W. Marshall and D.H. Wilkinson (Clarendon Press, Oxford, 1984).
[39] M. Bée, in: *Quasielastic Neutron Scattering* (Adam Hilger, Bristol/Philadelphia, 1988).
[40] S.A. Asher, Methods in Enzymology 76 (1981) 371.
[41] R. Kubo, J. Phys. Soc. Japan 17 (1962) 1100.
[42] S. Dietrich and W. Fenzel, Phys. Rev. B 39 (1989) 8873.